Applied Catalysis B: Environmental 234 (2018) 178–186

Contents lists available at ScienceDirect

Applied Catalysis B: Environmental

journal homepage: www.elsevier.com/locate/apcatb

Pressure dilution, a new method to prepare a stable Ni/fumed silica catalyst for the dry reforming of methane

V. Danghyan, S. Calderon Novoa, A. Mukasyan, E.E. Wolf*

Department of Chemical and Biomolecular Engineering, University of Notre Dame, Notre Dame, IN 46556, USA

ARTICLE INFO

Keywords:
Catalyst preparation by pressure dilution
Dry reforming of methane
Ni supported on fumed silica
Activity and stability

ABSTRACT

A novel method of catalyst preparation, using pressure dilution, which increased the dispersion and stability of a Ni/fumed SiO_2 catalyst is described. We first studied the effect of carbon formation on the activity and stability of Ni/fumed SiO_2 catalysts at different times on stream (TOS) during the dry reforming of methane (DRM). The catalysts were characterized by SEM/TEM and BET, XRD, XPS, TGA/DSC, and CO chemisorption. Catalysts prepared by impregnation of $Ni(NO_3)_2{\cdot}6H_2O$ onto fumed SiO_2, were subjected to various pretreatments which yielded high initial activities at 600 °C. The activation energy was measured to be 91 kJ/mol and the initial rate was of 8.5 [mol of CH_4/g_{Ni} h], comparable with Pt-Ni alloy catalysts. Depending on the pretreatment, however, the catalysts deactivated at different rates due to carbon formation. The carbon structure was studied by SEM/TEM and its amount measured by a carbon analyzer. We found that carbon accumulates mostly in the form of carbon nanotubes (C-NT) with Ni crystallites at the top, where the reaction takes place without affecting the activity during first hours of TOS. We also found formation of clumps of entangled C-NT with Ni crystallites encapsulated by the entangled C-NT, leading to loss of active area and deactivation.

A newly discovered method of catalyst preparation, referred as pressure dilution, resulted in a significant increase in Ni dispersion from 19% to 61%, when supported on fumed SiO_2. Moreover, Ni dispersion can be controlled by the pressure applied during catalysts' preparation. The higher dispersion resulted in a higher catalyst activity and increased stability towards carbon formation. A hypothesis of the re-dispersion process occurring during p-dilution is proposed.

1. Introduction

The reaction of CO_2 with methane or dry reforming of methane (DRM) produces syngas with a H_2/CO ratio close to 1, suitable for further methanol and Fischer-Tropsch synthesis [1,2]. DRM is environmentally more advantageous than other syngas production reactions since it utilizes methane and carbon dioxide, two major greenhouse gases [3].

In recent decades, many metal catalysts (Ni, Co, Pt, Ru, Rh, Pd, etc) supported on various oxides with different compositions and structures (SiO_2, La_2O_3, ZrO_2, TiO_2, CeO_2, Al_2O_3, MgO, etc) have been investigated [2,4–6]. However, few of them can be used in industry either for being too expensive (i.e. noble metals), difficult to prepare, and/or having low activity. Ni supported catalysts have been intensively investigated because they are price competitive, easy to prepare, exhibit good conversion rates, and are actually used in industry for steam reforming of methane [7–12]. Bradford and Vannice in 1999 [13] reviewed the literature on the DRM reaction and concluded that "according to most reports, the mechanism most consistent with experimental results, includes the following steps: reversible dissociation of CH_4 to yield CHx species and H_2, non-dissociative adsorption of CO_2 on the support, H-promoted CO_2 dissociation on the metal-support interface, reaction of CHx species with OH (or O) species to yield CH_xO species, and CH_xO decomposition on the metal-support interfacial region to yield CO and H_2", which highlights the complexity of the reaction.

One of the main limitations of using the DRM reaction on Ni catalysts is its deactivation due to the carbon formation. The type and structure of the carbon formed (carbidic, amorphous, polymeric, nanotubes, graphene type, shell-type, graphitic, filamentous), the amount deposited, and its effect on the catalyst activity have been investigated and found to be different for each catalyst and to depend on the metal-support interactions, catalyst structure, preparation method, reaction conditions, etc. [13–16].

On SiO_2 supported Ni catalysts, due to the weak metal-support interaction, Ni crystallites have high degree of reduction that results in

* Corresponding author.
E-mail address: ewolf@nd.edu (E.E. Wolf).

https://doi.org/10.1016/j.apcatb.2018.04.033
Received 18 November 2017; Received in revised form 14 April 2018; Accepted 17 April 2018
Available online 19 April 2018
0926-3373/

high initial activity, but also in favorable conditions for carbon formation, eventually resulting in catalyst deactivation [17]. The nature and type of deposited carbon have been studied, and some reports indicate that part of the carbon, referred as "reactive carbon, participates in the DRM reaction", but it can also block the active sites, referred as "inert or toxic carbon" [18,19] causing deactivation. Bychkov et al. [18] reported that initially, the deposited carbon blocks DRM activity, but eventually reacts with CO_2 reversing the deactivation under DRM conditions. These authors also report the formation of a secondary type of carbon that forms nanotubes with Ni particles located on their top. Kroll et al. [19,20] reported that on Ni/SiO_2 catalysts, as soon as methane contact the active sites, carbide-like species form, which are continuously fed by the dissociative activation of gaseous methane. This reactive carbon is readily oxidized into CO by oxygen atoms arising from the simultaneous carbon dioxide dissociation. Adsorption-desorption equilibrium ensure a fast interconversion between gaseous CO_2 and CO, as well as H_2O, which, when combined with the reversible activation of CO_2 and CO, leads to water–gas-shift equilibrium. These authors also report the formation of structured coke or graphite growing as hollow whiskers or carbon nanotubes (C-NT).

The formation mechanism of C-NT has also been intensively studied. In the case of week metal support-interaction, it has been found that the metal particle detaches from the support remaining on the top of the C-NT [15,21]. Several studies have shown that carbon nanotube's growth on Ni is related to crystallite size. Nanotubes start forming on Ni crystallites larger than 5 nm with the average size for the optimal growth being about 35 nm [22]. Gohier et al. [23] showed that during chemical vapor deposition of acetylene on Ni, carbon nanotube growth's mode switches from "base-growth" for smaller crystallites (< 5 nm) to "tip-growth" for large Ni crystallites (> > 5 nm).

Few papers have reported, however, on the relationship between the amount of C-NT formed during the DRM and the rates of catalyst deactivation. In most papers on DRM, results are reported at different operating conditions (temperature, GHSV, gas composition) and time on stream, and in fixed bed reactors under non-differential regime with very few studies reporting reaction rates, therefore it is difficult to compare catalytic activities.

Several reports have been published on methods to increase catalyst's stability by using special preparation procedures that embeds Ni on a surrounding structure, thus inhibiting carbon growth [24,25]. Depositing a SiO_2 overlayer on Ni crystallites yield catalysts with core-shell type structures that are coke resistant at 800 °C [26,27]. Similarly, Ni crystallites have been embedded inside highly porous alumina aerogels or zeolites thus limiting the space for carbon growth [28]. While such methods increase stability towards deactivation they also lower the activity due to the diffusion limitations. Lovell et al. [29] proposed a simple method of reduction-oxidation-reduction pretreatment to decrease Ni particle size and increase the metal dispersion, which resulted in an increase of methane conversion at 800 °C from 57% to 69% and better stability at 600 °C but at lower methane conversion.

The main objective of this work was to find the pathways between C formation, catalyst structure, and catalyst deactivation with the aim to develop catalysts with increased activity and stability. We carried out textural and bulk characterization of the catalysts (XRD and BET), as well as CO chemisorption, scanning and transmission electron microscopy (SEM and TEM), thermo gravimetric analysis (TGA) and differential scanning calorimetry (DSC), x-ray photoelectron spectroscopy (XPS), and carbon measurements at various TOS to determine the various factors affecting carbon deposition. Characterization results were correlated with conversion vs time on stream experiments and rate measurements to ascertain the relation between catalyst structure and Ni activity-stability.

Once such correlation was established, a novel, simple and very effective method of catalysts preparation combined with wet impregnation, referred as *pressure dilution* was discovered. This new method allowed us to increase significantly Ni dispersion, from 19% to 61%, which greatly improved catalyst's activity and stability towards carbon formation, which decreased deactivation. Emphasis is placed on the use of *fumed* SiO_2, because it is the key factor to understand the pressure dilution effect observed.

Table 1
BET area and Ni dispersion results for fresh catalyst's particles (pressed 10,000 psi) after different pretreatments.

Sample	Treatment	BET surface area, m^2/g	Metal dispersion
Fumed SiO_2	fresh powder	326	N/A
Fumed SiO_2	pressed particles	269	N/A
Regular catalyst (10%Ni content)	reduced-only	262	19%
	calcined-reduced	267	7%
P-diluted catalyst (5% Ni content)	reduced	276	61%
Regular catalyst (5% Ni content)	reduced	265	39%

2. Experimental procedures

2.1. Catalyst preparation

A 10%Ni on fumed SiO_2 catalyst was prepared by wet impregnation. 1.089 g nickel nitrate hexahydrate ($Ni(NO_3)_2{\cdot}6H_2O$, Alfa Aesar, 98%) was dissolved in water (~40 ml) and the solution was impregnated onto 2 g of fumed SiO_2 (Alfa Aesar, nominal surface area ~400 m^2/g, measured −326 m^2/g, Table 1). This mixture was dried at 70 °C on a hot plate with magnetic stirring (200 rpm) for 24 h and then dried again at 110 °C for 24 h without stirring. The resulting powder was then pressed (10,000 psi) crashed and sieved to obtain particles of about 1 mm in diameter, hereafter referred as *regular* 10% Ni/SiO_2 catalyst. One batch of powder was mixed with additional fumed SiO_2 (ratio 1:1) *before* pelletizing the mixture, a method referred hereafter as pressure diluted (p-diluted) catalyst with 5%Ni/SiO_2 content. The pelletized particles were crushed and sieved and then reduced before reaction.

2.2. Catalyst activity

Catalytic activity was measured in a continuous flow fixed bed quartz reactor (300 mm of length and 10 mm ID) at atmospheric pressure as previously described [30,31]. The fresh untreated catalyst (50 mg for regular catalyst and 100 mg for p-diluted catalyst filling a reactor volume of 0.15 cc) was loaded into the reactor and either directly reduced at 400 °C for 90 min in 5% H_2 (90 ml/min) referred as reduced-only catalyst, or first calcined in air (90 ml/min) at 600 °C for 5 h and then reduced at 400 °C with 5% H_2 (90 ml/min) denoted as calcined–reduced catalyst. After pretreatment, the reactor was purged with N_2 (50 ml/min), and the temperature was increased to the reaction temperature of 600 °C at a heating rate of 15 °C/min. Upon reaching 600 °C, a stream containing 20% CH_4, 20% CO_2 and 60% He was introduced at 120 cc/min corresponding to a gas hourly space velocity (GHSV) of 1440 L/g_{Ni} h for both regular and p-diluted catalysts. The GHSV is reported by g of Ni since we used catalysts with different % of Ni.

The composition of the effluent stream was measured using 2 gas chromatographs (GC). The first GC is equipped with an Alltech's CTR-I double packed column using 30 ml/min He as a carrier gas to separate CO_2, CO, CH_4. The second GC is equipped with a 6' molecular sieve 5 Å column in series with a 20' HAYSEP D column, using Ar as a carrier gas at 30 ml/min, and kept at 30 °C to separate H_2 and He.

CH_4 and CO_2 conversions and H_2/CO molar ratio were calculated as described in Eqs. (1)–(3) respectively, where F_i represents the molar flow rate of species *i*.

$$X_{CH_4} = \frac{F_{CH_4,in} - F_{CH_4,out}}{F_{CH_4,in}} \times 100 \quad (1)$$

$$X_{CO_2} = \frac{F_{CO_2,in} - F_{CO_2,out}}{F_{CO_2,in}} \times 100 \quad (2)$$

$$\frac{H_2}{CO} = \frac{F_{H_2,out}}{F_{CO,out}} \quad (3)$$

Reaction rates were calculated under differential reaction conditions (i. e. $X_{CH_4} < 15\%$) by multiplying the molar flow rate of methane by the conversion divided by the weight of Ni loaded into the samples.

2.3. Catalyst characterization

The catalyst's bulk structure was determined by X-ray diffraction (XRD) in a Bruker diffractometer (D8 Advance) using Cu Kα radiation, at 40 kV and 40 mA. The step-scan size of 0.02° and counting time of 1 s was used for the angular range of 20–80° (2θ).

Textural characterizations such as BET surface area, pore volume, and pore size distribution for fresh catalysts were measured in a Micromeritics ASAP 2020 adsorption apparatus after being vacuum degassed for 16 h at 130 °C. The Ni surface area and dispersion were determined in the same instrument by CO chemisorption. Samples were first pretreated in-situ in hydrogen flow at 400 °C for 90 min. After cooling to 35 °C, CO chemisorption was performed at that temperature with the CO pressures between 100 and 350 mbar. Dispersion was calculated from CO chemisorption assuming crystallites were hemispherical and a 1:1 stoichiometry and that the crystallites were reduced.

A TGA-DSC apparatus (Mettler-Toledo) was used to perform in-situ thermogravimetric analysis. About 30 mg of untreated fresh catalyst was placed on the heating stage and heated to 400 °C at a rate of 15 °C/min in either, nitrogen, air, or 5% H_2 (balance N_2) at 50 ml/min. In each case, after reaching 400 °C, the temperature was kept constant for 1 h.

An FESEM Magellan 400 (FEI) field emission scanning electron microscope (SEM) was used to image the catalysts. Spent catalysts were also imaged using a FEI Titan 80–300 transmission electron microscope (TEM) with a point-to-point resolution of 0.19 nm with information limit below 0.1 nm. Cross sections of carbon tube clumps were obtained using Helios NanoLab DualBeam 600 (FEI) SEM/FIB workstation.

X-ray photoelectron spectroscopy (XPS) measurements were carried out in a PHI Versa-Probe II spectrometer, using Al Kα radiation at 1486.6 eV under high power mode. A Multipak software package was used to de-convolute the spectral peaks and determine relative elemental surface concentrations.

The amount of carbon in the catalysts was measured in a Costech ECS 4010 elemental C analyzer equipped with a specialized gas chromatograph (GC). Acetanilide (71.09% carbon content) was used as a calibration standard.

3. Results and discussion

XRD patterns of fresh catalysts prepared by wet impregnation after various pretreatments (Fig. S1a) show that the reduced-only catalyst exhibits XRD lines at 2θ = 44.2, 51.4 and 76.2°, corresponding to metallic Ni, with crystallite sizes in the 5–30 nm range as determined by SEM (Fig. S2A). The XRD pattern of the calcined catalyst (Fig. S1b), has lines at 2θ = 37.0, 43.0, 62.6, 75.2 and 79.2° corresponding to NiO. The calcined-reduced catalyst exhibits an XRD pattern corresponding to metallic Ni (Fig. S1c), but with crystallite sizes in the 25–60 nm size (Fig. S2B) range due to sintering at the relatively high calcination temperature used (600 °C).

BET surface area values for catalysts after different pretreatments are presented in Table 1. Regardless of wet impregnation, dilution, reduction and calcination-reduction pretreatments all catalysts exhibit similar surface areas.

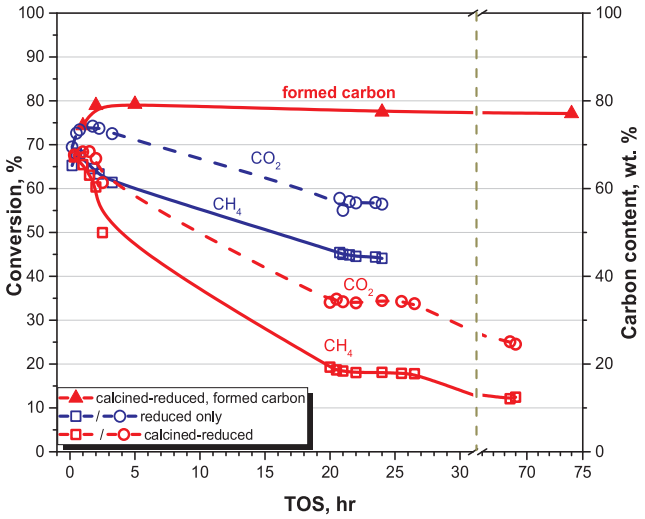

Fig. 1. CH_4 and CO_2 conversions vs TOS for reduced-only and calcined-reduced samples at 600 °C along with the formed carbon amount at different TOS for calcined-reduced catalyst.

Pressing the fresh impregnated powders to form pellets at 10,000 psi is the main factor decreasing the surface area. This is confirmed by the surface area of un-impregnated fumed SiO_2 before and after pelletizing, which decreases from 326 m^2/g to 269 m^2/g, similar to the values obtained for the impregnated catalysts (Table 1).

Ni dispersion results calculated from CO chemisorption are also listed in Table 1. The calcined-reduced catalyst exhibits the lowest dispersion due to partial sintering at 600 °C during calcination. For reduced-only catalysts, dispersion is higher than on the calcined-reduced catalysts, but it is the highest at 61% for the pressure-diluted catalyst. Even higher dispersion was obtained at 5000 psi, as shown later in Fig. 7.

Methane and carbon dioxide conversions vs time on stream (TOS) for reduced-only and calcined-reduced catalysts are shown in Fig. 1. For both pretreatments, conversion reached a maximum at the beginning of the run (82% equil. methane conversion [32]) and remained nearly constant for the first 1–2 h, then decreased with TOS, with the calcined-reduced catalysts deactivating at a higher rate. The activation energy for the reduced catalysts during 1 h TOS was 91.1 kJ/mol, similar to the values reported in the literature [33]. The reaction rate of 8.5 [mol of CH_4/g_{Ni} h], measured at lower temperatures to reach differential conditions, but at a GHSV of 1440 L/g_{Ni} h is fairly high for Ni, resulting in the high conversions at 600 °C reported here. For comparison, in the case of the noble metal catalyst Pt/ZrO_2 the reported reaction rate is in the range of 14–17.4 [mol of CH_4/g_{Pt} h] [34].

To ascertain the effect of diffusion on the kinetics, we calculated the Weiz-Prater observable and substituting the proper numerical values (see Table S1) obtained a value of 0.3, indicating that diffusion is not limiting the reaction rate at 600 °C [35]. There is a discrepancy between methane and CO_2 conversion, as it is usually reported for this reaction [36,37]. The difference is partly due to the carbon deposition mainly from methane, as it will be shown later, and possibly due to the reverse water-gas shift reaction [37].

The calcined-reduced catalyst deactivated faster because of its lower Ni dispersion compared to the reduced-only catalyst (Table 1). It has been reported that short reduction-oxidation-reduction cycles of already calcined catalysts help to increase the metal dispersion [29,38]. According to our results, the initial calcination treatment significantly decreases the metal dispersion, which can be avoided by using the reduction-only pretreatment. The pretreatment used in different runs was related to the deactivation time, which was faster using the calcined-reduced pretreatment leading to shorter runs.

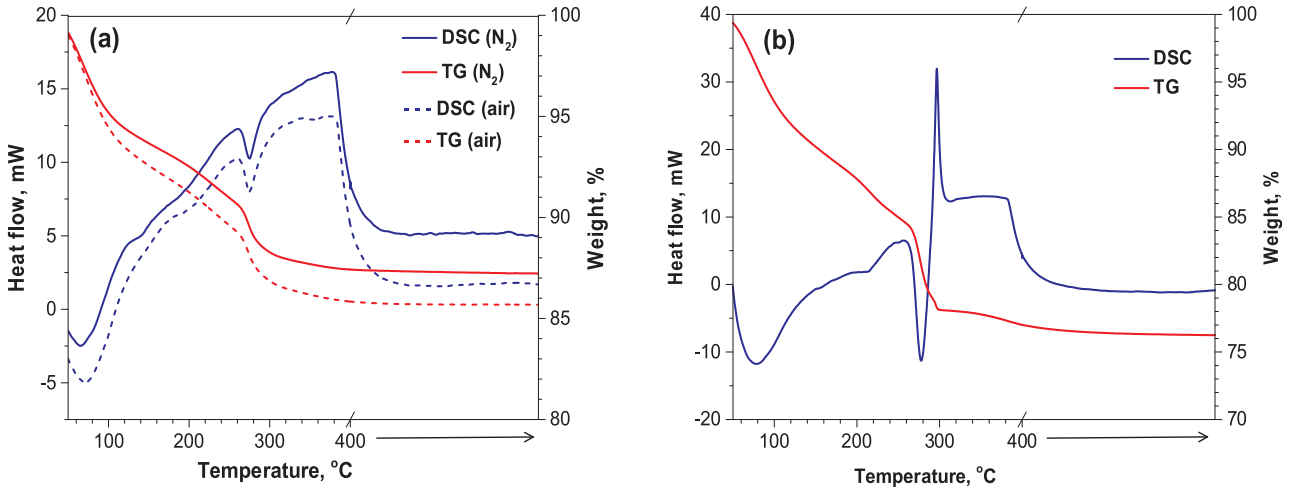

Fig. 2. TGA-DSC results for impregnated powders: (a) N_2/air flow, (b) 5%H_2 flow.

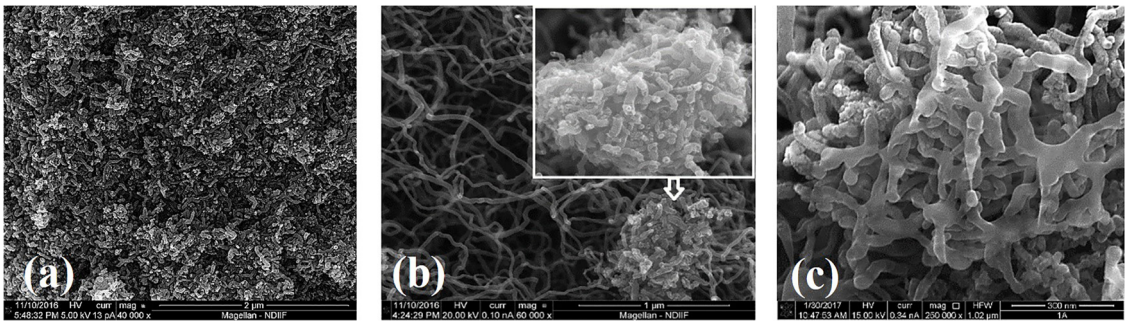

Fig. 3. SEM images of deactivated catalyst: entanglement of carbon nanotubes (a) and (b), cross section of C-NT clump (c).

The effect of pretreatment is further explained by the TGA-DSC results shown in Fig. 2a–b for the impregnated $Ni(NO_3)_2{\cdot}6H_2O/SiO_2$ particles obtained under different gas atmospheres. In a non-reducing atmosphere (air and N_2, e.g. calcination step) there is ~10% continuous decrease in weight (Fig. 2a) in the temperature range of 50–260 °C, corresponding to a gradual loss of 4 molecules of water out of six [39]. A steep decrease in weight occurs at about 260 °C, which is close to the decomposition temperature of $Ni(NO_3)_2{\cdot}2H_2O$, along with a decrease in heat flow, corresponding to the endothermic decomposition of nickel nitrate to NiO [39]. The reduction of NiO by hydrogen as in the calcination-reduction pretreatment, is also an endothermic process, which starts slowly at about 120 °C and is completed at about 320 °C, showing featureless TGA-DSC curves (Fig. S3).

Fig. 2b shows that a different process occurs during decomposition/reduction in H_2. While the shape of the weight change trace is similar to the ones registered in N_2 or air atmospheres, the DSC results show that at the decomposition temperature of $Ni(NO_3)_2{\cdot}2H_2O$ in H_2, there is a combination of endothermic and exothermic processes.

In the case of Fig. 2b, results with the reduced-only catalyst are shown to amplify the exothermic effect. We interpret this effect as evidence of the endothermic decomposition of Ni nitrate followed by exothermic reactions between its decomposition products and H_2. Similar studies of bulk nickel nitrate decomposition show that at ~250 °C the main gaseous product is N_2O, which could react exothermically with H_2 [40]. The exothermic effect (temperature increase) and the presence of H_2 enables rapid reduction of NiO, formed during nitrate decomposition, to metallic Ni. As will be discussed later, compared to the endothermic processes observed during calcination-reduction pretreatment, this endothermic-exothermic single step reduction process results in increased dispersion of Ni crystallites for reduced only catalysts. The TGA/DSC and dispersion results indicate that the difference in the rate of catalyst deactivation is related to the metal crystallite size i.e. dispersion, and its distribution on the support, which in turn is affected by pretreatment.

The percentage of carbon formed at different TOS at 600 °C for calcined-reduced catalyst is also presented in Fig. 1. Carbon elemental analyzer measurements show that after only 1 h of TOS the amount of formed carbon reaches 74 wt.%, attains a maximum of about 79 wt.% after 2 h TOS, and thereafter remains nearly constant with TOS. To accommodate this much carbon the catalyst's bed volume doubles, and even though the conversion of methane is continuously decreasing, it is still around 14% after 70 h of TOS. The C deposition results for the reduced-only catalysts are similar, but the rate of carbon deposition at short TOS is not as steep.

The relatively high methane conversion at TOS > 1 h begs the question of how it is possible to have an active Ni surface in the presence of so much carbon. The answer becomes clearer in the SEM micrographs, shown in Fig. 3, of the calcined-reduced catalyst after 24 h TOS (CH_4 conversion ~20%). Fig. 3a and b show the formation of carbon nanotubes (C-NT) with Ni crystallites appearing as bright spots located at the top of C-NT. Following the various interpretations of the DRM reaction pathways [18,19], it can be assumed that methane decomposition takes place on sites located at the interface of C-Ni crystallites located at the top of the C-NT forming Ni-carbide sites.

The growth of C-NT is fast during the first hours of TOS reaching a maximum in C content, but then it stabilizes with TOS, in agreement with Kroll et al. [19],

CH_4 and CO_2 react at the interface of Ni-C-NT leading to the formation of CO and H_2, which start decreasing slowly with TOS. The image in Fig. 3b, at higher magnification (125,000×), shows that in certain areas, there are clumps of entangled C-NT. A further magnified image (250,000×) of the cross section of a clump, shown in Fig. 3c, was

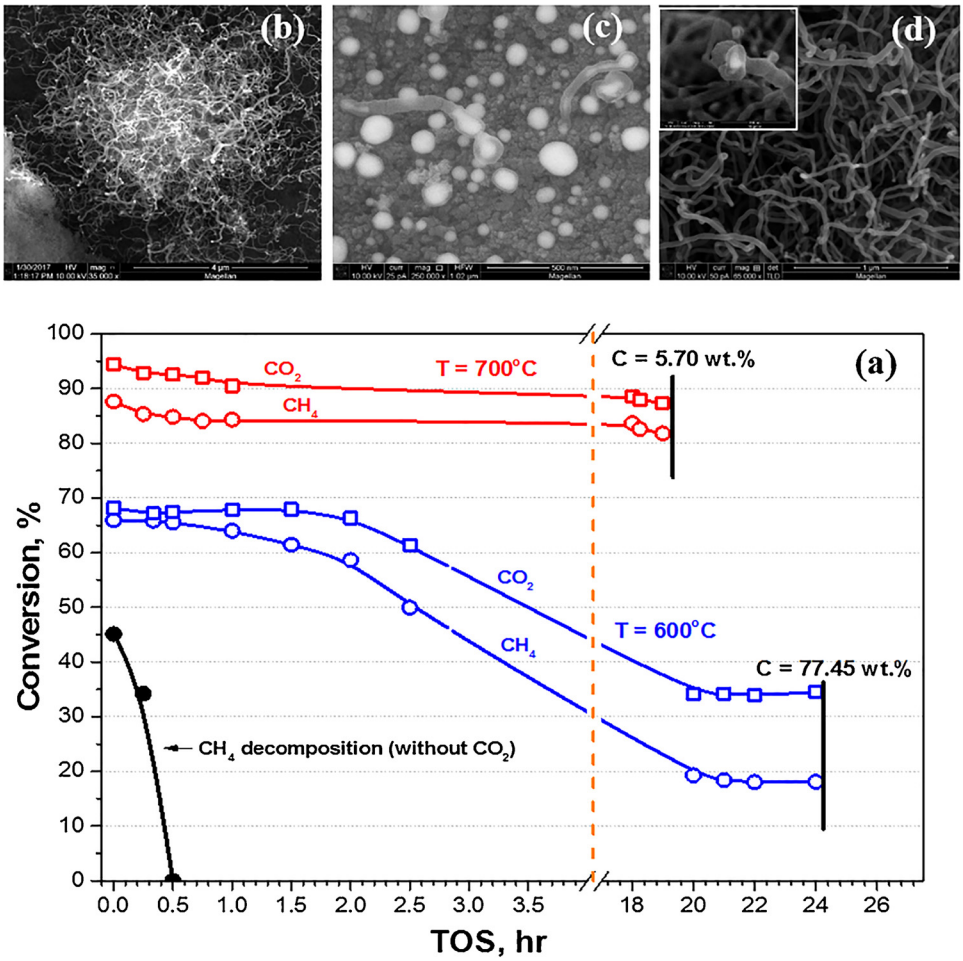

Fig. 4. a) CH_4 and CO_2 conversions during DRM for calcined-reduced catalysts at 600 and 700 °C and CH_4 decomposition (without CO_2) at 600 °C along with SEM micrographs of spent catalysts: (b) DRM at 600 °C, (c) DRM at 700 °C, (d) CH_4 decomposition (no CO_2) at 600 °C.

obtained by cutting it with a focused ion beam (FIB). This image shows that the clump still retains some porous structure but Ni crystallites are now encapsulated within neighboring entangled C-NTs. Thus we attribute deactivation to the loss of Ni active area due to encapsulation in these clumps.

Fig. 4 shows methane and CO_2 conversions vs TOS on calcined-reduced catalysts at 600 °C and 700 °C, during the DMR and methane decomposition (without carbon dioxide). Also shown are representative SEM micrographs of the catalysts at different TOS and conditions, as well as the amount of C measured at the end of the run after 24 h and 19 h TOS at 600 °C, and 700 °C respectively. During the DRM reaction, CH_4 conversion at 600 °C decreases to 20% after 24 h TOS, with 77 wt. % of carbon formation.

The SEM micrograph of the spent catalyst (Fig. 4b) shows the formation of large amounts of entangled C-NT with Ni crystallites embedded in the entangled C-NT

rather than at their top. It appears that as more C-NT form, Ni crystallites in adjacent C-NT become in contact resulting in their encapsulation by both C-NTs.

At 700 °C (Fig. 4a), the initial conversion is higher, as expected (92% conversion at equilibrium), but no significant deactivation is observed with only 5.7% of carbon formation after 19 h TOS, showing that C formation (or lack of it) correlates with increasing or decreasing rates of deactivation. It should be noted that the equilibrium amount of C formation is lower at 700 °C than at 600 °C (the equilibrium molar ratio of C at 600 °C and 700 °C is 1.6 [4]), which further contributes to the increased stability. The corresponding SEM micrograph in Fig. 4c, shows larger crystallites than at 600 °C with only a few a C-NT formed. This confirms that the decrease in C-NT formation and the lack of entanglement decreases deactivation.

Conversion during CH_4 decomposition (without CO_2 present) at 600 °C is also shown in Fig. 4 for the 10% Ni/SiO_2 reduced-only catalyst. The reduction only pretreatment was used to be able to observe the rapid deactivation occurring during this reaction, even on the catalyst having the highest Ni dispersion. Methane conversion during its decomposition falls rapidly and the catalyst is completely deactivated after 30 min of TOS, compared with the relatively low deactivation rate occurring during the DRM in that short time period. The corresponding SEM micrograph of the spent catalyst (Fig. 4d) shows significant formation of C-NT, as in the DRM reaction. The higher magnification SEM insert (Fig. 4d) shows Ni particles encapsulated within C-NTs leading to loss of Ni interfacial area and thus to the rapid deactivation observed during methane decomposition.

Borowiecki [42], and several later studies [41,43,44], showed that C-NTs form on Ni crystallites with sizes in the 5–160 nm range during methane dry reforming, methane steam reforming, and methane decomposition. C-NTs have also been reported to form in several transition metals such as Fe, Co, Cu with their structure depending on the C deposition reaction, support, and operating conditions used, in particular, temperature (> 400 °C). Previous work in our group during ethanol decomposition on Ni supported on silica and ceria [46] at temperatures in the range of 250–300 °C, found that for that reaction, deactivation occurs via the formation of C layers on top of Ni crystallites, and not via C-NT encapsulation.

The results presented in Fig. 4 also show that the presence of CO_2 in the DRM reaction decreases the rate of C-NT encapsulation by reacting

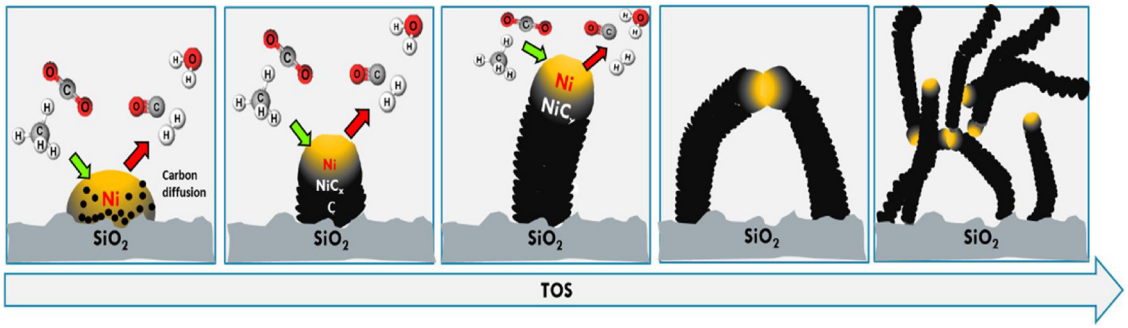

Scheme 1. Model of C-NT growth during DRM reaction and encapsulation andentanglement.

with Ni-C-NT sites, in agreement with previous models [14,15]. This reaction limits the growth rate and the linking of adjacent C-NTs, and thus Ni encapsulation, decreasing the rate of deactivation during the DRM compared with methane decomposition. A CO_2 decomposition experiment (without methane) showed no carbon deposition at 600 °C.

Following schemes proposed in the literature [23,43,44,45,47], a model of C-NT formation is presented in scheme 1. Our contribution to the understanding of the activity and deactivation of the Ni/fumed silica catalyst described so far, has been to show the relation of the C-NT formation and their entanglement, with the rate of deactivation during the DRM reaction.

To observe the deactivation process in a shorter TOS, we decreased the amount of catalyst used. To prevent non-uniform catalyst distribution in the bed, and minimize the formation of channeling or voids we diluted the catalysts with silica. We first run the reaction using standard *bed dilution of the* regular 10% Ni/SiO_2 catalyst particles with additional fumed SiO_2 particles in a 1:1 relation, so the amount of Ni was actually 5% (Fig. 5). As previously mentioned, to prevent diffusional limitations, all catalysts were used in the form of particles with sizes of less than 1 mm, which were obtained by pressing wet impregnated and dried powders to 10,000 psi to form a pellet that was later broken and sieved into small particles. Based on the effect of pressure on the fumed silica BET area (Table 1) we decided to alter the preparation by first mixing the dried wet-impregnated catalysts with fumed SiO_2 in a 1:1 ratio, ***before pressing the diluted*** mixture to 10,000 psi and then broken it into small particles. This catalyst, referred hereafter as p-diluted catalyst, also contained 5%Ni. The p-diluted catalysts particles were then loaded into the reactor and pretreated as in previous runs by reducing them *before* reaction.

Results obtained during the DRM reaction on various diluted catalyst using the same total amount of Ni and operating conditions (i.e. GHSV = 1440 L/g_{Ni} h, 600 °C) are shown in Fig. 5a. The p-diluted catalyst exhibited a similar methane conversion (68%), than the undiluted ones, but most significantly, it did not deactivate (~1–2% conversion decrease) during the entire run of 40 h TOS. Fig. 5a also shows that the undiluted reduced-only 10%Ni/SiO_2 catalyst has almost the same initial methane conversion (67%) as the p-diluted catalyst, but it starts deactivating after ~2 h TOS with conversion decreasing to about 25% after 20 h TOS. Conversion results, obtained on a standard *bed* diluted catalyst, i.e. 10% Ni regular impregnated catalyst particles diluted with fumed SiO_2 particles but not pressed, show that it decreased by 25% after 23 h TOS. Likewise, an undiluted 5% Ni/silica prepared by wet impregnation only deactivates, to about 53% conversion after 24 h TOS. As before, when applying the calcination-reduction pretreatment to the p-diluted catalyst, it deactivates at a higher rate compared to the reduced-only p-diluted catalyst, with methane conversion decreasing by 15% after 20 h TOS (not shown).

SEM and TEM images at the top of Fig. 5 (Fig. 5b, c) of the spent p-diluted catalyst show fewer C-NT with bright spots). The TEM/STEM image (Fig. 5d), clearly shows metallic Ni crystallites in the bright field as well as in the STEM image of the same C-NT (Fig. 5e). This indicates again that the lower rate of deactivation of the p-diluted catalysts is due to a low concentration of C-NT formed and thus subsequent low rate of entanglement and therefore low rate of deactivation. STEM

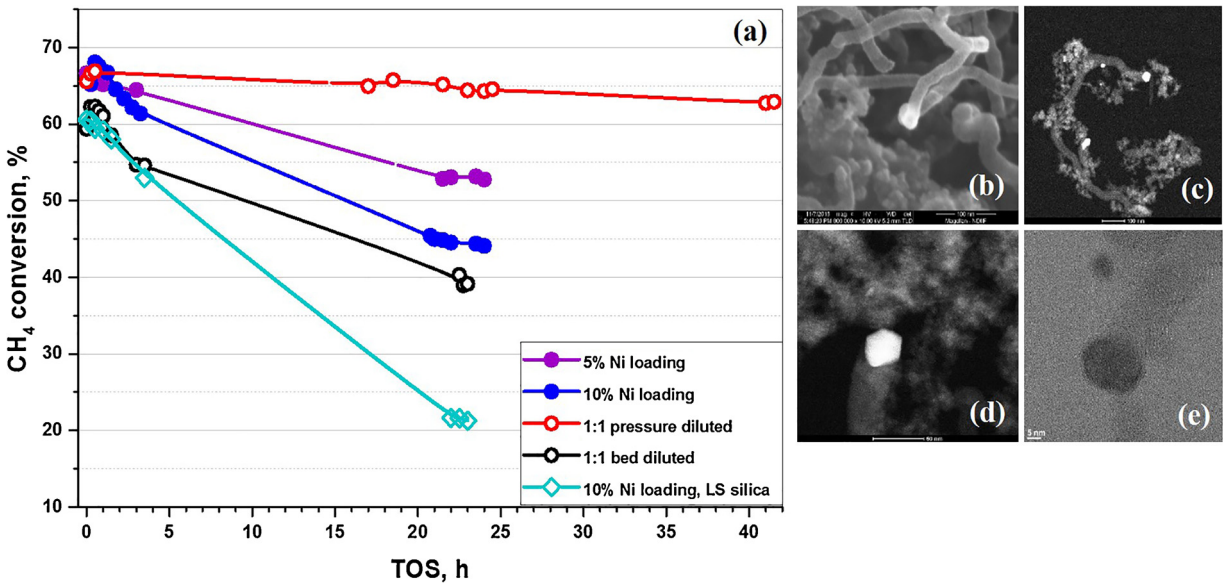

Fig. 5. Methane conversion during DRM at 600 °C for 5 and 10% Ni loaded, p-diluted and bed diluted fumed SiO_2 and 10% Ni loaded low surface area (LS) SiO_2 catalysts and SEM, TEM and STEM images of the p-diluted catalyst after 40 h TOS.

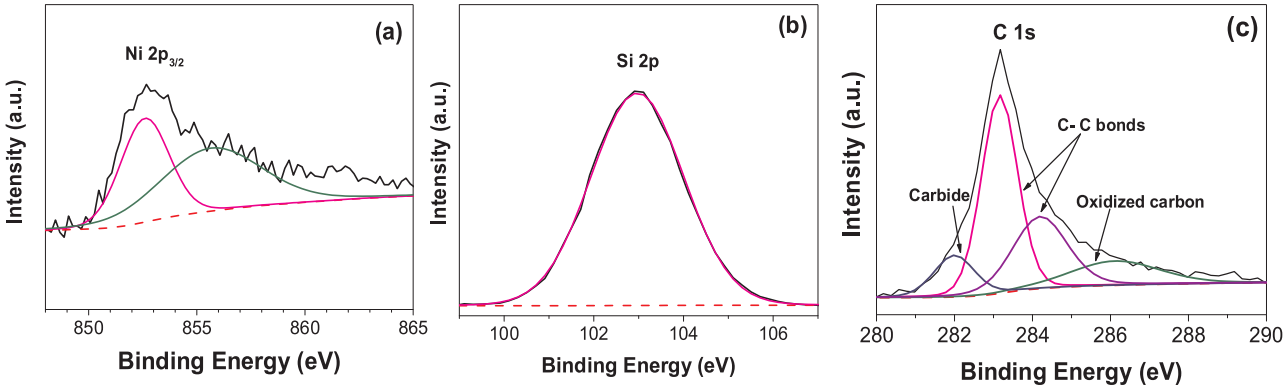

Fig. 6. XPS results of (a, b) fresh, and (c) deactivated catalysts.

micrographs after 1 h show that the distribution of crystallites in the p-diluted catalyst does not change significantly (less than 5 nm). Likewise, in the calcined-reduced catalyst crystallites are initially large (30–60 nm) and do not change that much after 1 h of reaction.

Fig. 6a–c shows XPS results of the Ni $2p_{3/2}$ and Si 2p signals of the fresh catalyst as well as the C1s signal of the deactivated catalyst after 21 h TOS. The Ni $2p_{3/2}$ signal of the fresh reduced–only catalyst (Fig. 6a) is relatively small, and exhibits a peak at 852.8 eV corresponding to reduced Ni, and a broader peak at around 857 eV, which can be ascribed to surface oxidized Ni. In these XPS studies the catalysts were first reduced ex-situ in the flow reactor, and then transferred to the XPS chamber with some exposure to air. Even though the samples were cleaned by plasma etching before XPS analyses, exposure to air, albeit brief, might have caused some surface oxidation resulting in some surface NiO formation, shown in the Ni $2p_{3/2}$ XPS signal.

We also attribute the small Ni $2p_{3/2}$ XPS signal to the fact that Ni is dispersed into the fumed SiO_2 pores, therefore only photoelectrons on the small fraction of crystallites located on the external surface of the catalysts samples can escape into the vacuum chamber for detection and analysis. Fig. 6b shows the large Si 2p signal at a BE of 103 eV corresponding to Si^{+4} for the p-diluted catalysts, which are similar to the undiluted regular catalyst (not shown), indicating that the p-dilution process does not alter the SiO_2 structure.

The large XPS C1s signal of the catalyst after 1 h TOS (Fig. 6c) corresponds to 82% of the overall surface concentration, which is in agreement with the total amount of carbon measured by the elemental C analyzer. The C1s signal can be deconvoluted into four peaks, with the two large peaks at 283.5 and 284.7 eV corresponding to the formation of C—C bonds in C-NT [48]. A smaller peak at around 286.5 eV corresponds to oxidized carbon species, probably formed at the support-C interface, and a small peak at 282 eV, can be attributed to the formation of Ni carbides that can form at the Ni-C NT interface at the top of the C-NT [49]. Overall, XPS results are in agreement with the other characterization results and show that the oxidation state of Ni does not play a significant role in deactivation, further supporting our assumption that C-NT entanglement is the main cause of loss of active Ni area leading to deactivation.

The formation of C-NT is related to the crystallite size and can be suppressed by designing a catalyst with crystallites that does not lead to the formation of C-NT at the reaction conditions used. It should be noted that different types of C-Ni sites are formed on the Ni crystallites at the top of the C-NT, and we cannot ascribe the activity to specific sites. Based on literature reports and our results, it can be assumed that the number of active sites correlates with the interfacial area of the Ni crystallites at the top of the C-NT, which is reduced by entanglement, leading to deactivation.

It remains to explain the effect of p-dilution in exhibiting high activity and low deactivation rate of these catalysts. BET results (Table 1) show that pressure alone alters the surface area of the fumed silica used, but XPS results showed that it remains as SiO_2.

Fumed SiO_2 has a very different structure than the co-precipitated one, as it is produced from the flame pyrolysis of tetraorthosilicate. A model of the growth processes in flames, proposed by Schaefer and Hurd [50], envisions the initial formation of rough primary particles with fractal geometry, which aggregates into highly ramified clusters. These authors identify four main processes that determine the structure of the final powders: kinetic nucleation, ballistic polymerization, sintering, and diffusion controlled aggregation.

According to the BET results (Table 1), fresh fumed SiO_2 is compressible, as shown by the decrease in surface area after pressing it to form a pellet and then particles. During the preparation process of p-diluted catalysts, when impregnated fumed SiO_2 (containing Ni $(NO_3)_2{\cdot}6H_2O$) is mixed with fresh fumed SiO_2 and then pressed, we assume that pressure brings the added fresh fumed SiO_2 closer and in direct contact with impregnated SiO_2.

CO chemisorption results listed in Table 2, along with Ni dispersion, show that p-diluted catalyst exhibits 61% dispersion, the highest from all the catalysts prepared in this work. The increase dispersion indicates that Ni was transferred from the undiluted particles to the additional surface area provided by the fumed SiO_2 layer in direct contact with it. Such transfer does not occur when the catalyst is diluted in the flow reactor by adding the same amount of fumed silica to the undiluted catalyst without using pressure.

In the diluted bed, fumed silica is not in a very close contact with the undiluted regular catalysts as in the p-diluted catalyst, and thus Ni is not transported into the added fumed silica, without affecting dispersion. This is confirmed by the Ni dispersion results measured after applying different pressures during the preparation of p-diluted catalysts. Fig. 7, shows that even pressing the initial powder at 1000 psi, Ni dispersion in the final catalyst increases more than twice to about 47%. The maximum dispersion of 67% is observed when pressing the

Table 2
Ni dispersion results calculated by CO chemisorption for catalyst samples prepared with fumed and co-precipitated SiO_2.

Catalyst	Pressing pressure	Metal dispersion	Calculated crystallite size
Fumed SiO_2 (~320 m^2/g), 10 wt.% Ni	N/A (powder)	18.5%	5.5 nm
	10,000 psi	19.4%	5.2 nm
Fumed SiO_2 (~320 m^2/g), 5 wt.% Ni	10,000 psi	39.2%	2.6 nm
Fumed SiO_2 (~320 m^2/g), p-diluted	10,000 psi	61.2%	1.7 nm
Co-precipitated SiO_2 (~200 m^2/g), 10 wt.% Ni	10,000 psi	18.8%	5.4 nm
Co-precipitated SiO_2 (~200 m^2/g), p-diluted	10,000 psi	17.8%	5.7 nm

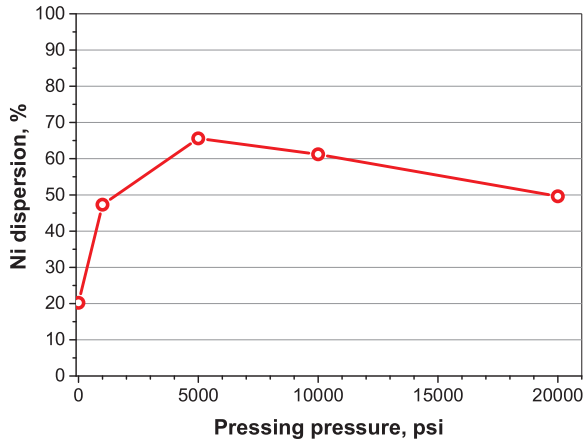

Fig. 7. Effect of pressing pressure on the final Ni dispersion during preparation of p-diluted catalysts.

particles at 5000 psi, which suggest that at this pressure, the newly incorporated fumed silica is located at the optimal distance, from the impregnated fumed silica to facilitate Ni transport to the added fumed silica. Further increase in the pressure decreases dispersion, possibly due to diffusion limitations during Ni transfer.

In addition to the chemisorption results, TEM/STEM analyses also confirm the re-distribution of Ni crystallites in p-diluted catalysts. Fig. 8a and b show images of regular and p-diluted freshly prepared catalysts. The undiluted regular catalyst contains a larger fraction of large Ni crystallites (appearing as bright spots) compared to the p-diluted one. Using contrasted-trehsolded images at higher magnification, the Ni crystallite size distribution shows that in the case of the p-diluted catalyst, the total fraction of Ni crystallites with sizes < 4 nm is about 70% (Fig. 8d), whereas in the case of regular catalyst it's around 45% (Fig. 8c).

For p-diluted catalysts there are very few Ni crystallites of 15 nm, but for regular undiluted catalysts the fractions of crystallites > 15 nm is about 35%. When we repeated the p-dilution preparation using regular co-precipitated SiO_2 (Sigma Aldrich, nanopowder silica with 180–225 m^2/g surface area), the increase in dispersion and stability observed on Ni supported on fumed SiO_2 catalyst were not observed (Fig. 5 and Table 2). Therefore, the fumed SiO_2 structure plays an important role in the increased dispersion due to pressure dilution.

A couple of processes can be proposed to explain the transport of Ni in the p-diluted catalyst resulting in increase dispersion: one via transport of the quasi-melted precursor, and the other by gas phase transport during reduction. Ni nitrate has low melting point (56.7 °C for hexahydrate, 85.4 °C for tetrahydrate and 181 °C for dihydrate [51]) and during drying, the impregnated catalysts were heated to 110 °C. It follows that the $Ni(NO_3)_2$ precursor can be in the form a quasi-liquid melt (see Fig. 2) and such phase can spread on the added fumed SiO_2 layer. Upon reaching the decomposition temperature of $Ni(NO_3)_2$, and further reduction, smaller crystallites of Ni can form, leading to higher dispersion. The second possible transport mechanism is via gas phase diffusion of the gas phase species formed during the decomposition/reduction pretreatment, which can be deposited into the added silica layer. Banerjee and Crozier [52], using in-situ TEM, studied in great detail the Ni deposited on large non-porous SiO_2 spheres (80–400 nm). They used a similar wet impregnation process as in our work with a Ni

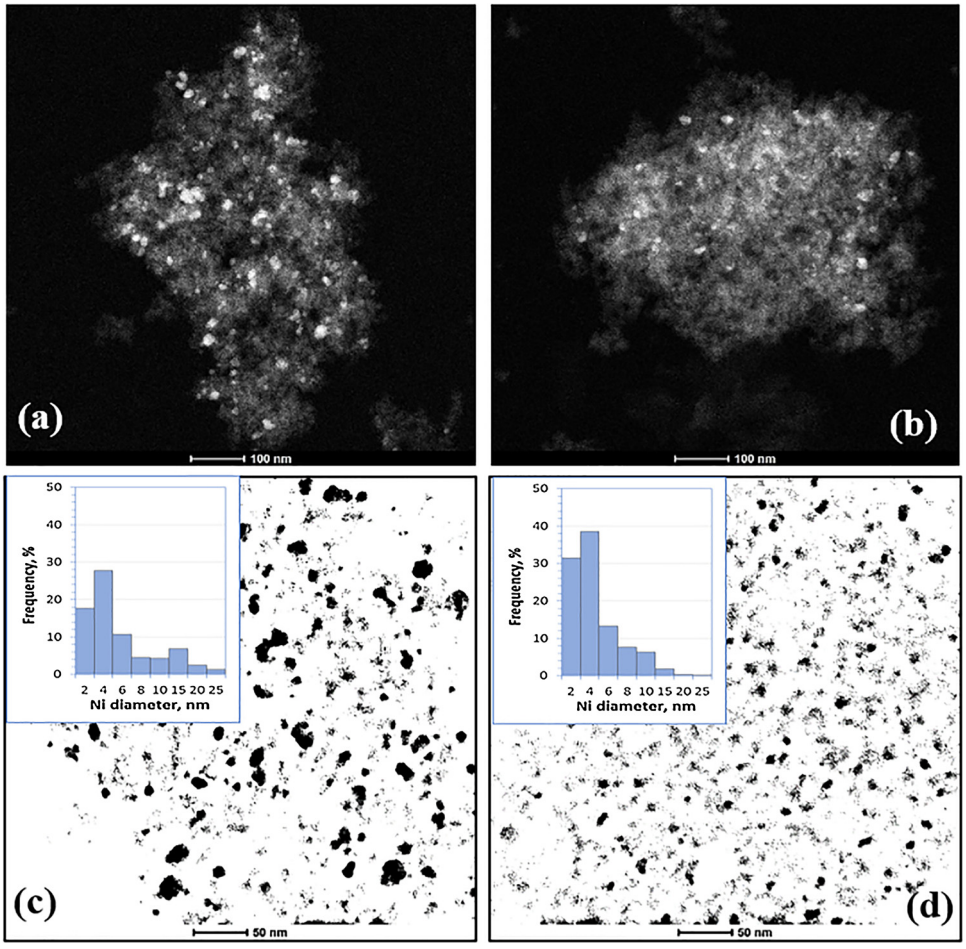

Fig. 8. STEM images along with contrasted & thresholded images of regular (a, c) and p-diluted (b, d) fresh catalysts and calculated Ni crystallite size distribution.

$(NO_3)_2$ precursor dissolved in ethanol, pretreating them by calcination at 300 °C and reduction at 400 °C. They report, that in their model catalysts, no spreading took place during calcination and that significant gas phase transport occurred during direct reduction of the precursor, in agreement with our reduction-only results. The precursor liquid in that work accumulated mainly in between the large SiO_2 spheres' point of contact, which is very different than in our porous fumed silica. In our case the uptake of the solution is mainly due via capillary forces, leading to selective adsorption of the precursor salt on sites within the fumed silica pores. No local temperature increase due to pressure were observed, and except for the decrease in BET area with pressure, no other mechanical factors can cause the re-dispersion of the active phase observed after pressing. A detailed model of the processes leading to the increase in dispersion by p-dilution for fumed SiO_2, is presented in the graphical abstract.

We are not aware of another catalyst preparation method involving pressure dilution, resulting in higher dispersion and a patent disclosure has been submitted. It should be emphasized that p-dilution is valid for the specific conditions used in preparing the catalysts and may not be applicable to other catalyst systems, depending on the metal precursor, support, and preparation procedure used. Further work is being conducted in our group to determine the key factors involved in pressure dilution, but clearly the use of fumed silica is one of them.

4. Conclusions

Ni/SiO_2 catalysts prepared by wet impregnation of fumed SiO_2 with $Ni(NO_3)_2{\cdot}6H_2O$ were pretreated in-situ by H_2 reduction-only (400 °C) and by air calcination (600 °C)-reduction. TGA/DSC results indicate that reduction only pretreatment results in endothermic decomposition combined with exothermic reduction of $Ni(NO_3)_2{\cdot}6H_2O$, and endothermic decomposition only for the samples calcined in air. These two treatments yield catalysts with the same initial activity but different rates of deactivation, with the calcined-reduced catalyst deactivating faster than the reduced-only catalysts. The catalysts were stable for the first hour but then deactivated with TOS. The initial methane conversion was quite high, 68–70% during 30–60 min TOS at 600 °C, and the initial rate of 8.5 (mol of CH_4/g_{Ni} h) and activation energy of about 92 [KJ/mol], are comparable with catalysts containing Pt-Ni alloys.

Carbon deposition takes place during the DRM reaction on Ni/fumed SiO_2 catalysts in the form of C-NT with the Ni crystallites atop of the C-NT, a well-known mechanism of C-NT formation. C-NT formation allows deposition of large amounts of carbon on the catalyst (up to 78%), with the reaction taking place on the interface of C-NT on the Ni crystallites atop the nanotubes. We also found that C-NT form clumps of entangled C-NT that eventually encapsulate the Ni crystallites leading to catalyst deactivation. Similar C-NT structures form during methane decomposition (without CO_2), but at a much faster rate leading to complete deactivation in about 30 min. This shows the main source of carbon formation is methane, and indirectly to the conclusion that CO_2 slows down C-NT formation either reacting with carbon or by blocking sites for methane decomposition.

A novel method of catalyst preparation was discovered by diluting the impregnated catalysts with fumed SiO_2 support, then applying pressure, using a press, to the mixed powder to form a pellet, which is then broken into particles. The p-diluted catalysts exhibited higher dispersion that varies with the applied pressure, showing an optimal dispersion of 67% at 5000 psi. A transport mechanism of Ni $(NO_3)_2{\cdot}6H_2O$ into the added silica was proposed to explain the increased dispersion.

Because of their higher dispersion, p-diluted catalysts showed increased activity and stability than the best undiluted catalyst. The higher stability was due the formation of fewer C-NTs, located far from each other, resulting in decreased entanglement.

Acknowledgements

We gratefully acknowledge the support of this work by grant NPRP-8-509-2-209 from the Qatar National Research Fund (member of the Qatar Foundation). The statements made herein are solely the responsibility of the authors. We also acknowledged the use of the following Facilities of the University of Notre Dame: Notre Dame Integrated Imaging Center (NDIIC), Notre Dame Materials Characterization Facilities (MCF), and Notre Dame Center for Environmental Science & Technology (CEST).

Appendix A. Supplementary data

Supplementary material related to this article can be found, in the online version, at doi:https://doi.org/10.1016/j.apcatb.2018.04.033.

References

[1] M.E. Dry, Catal. Today 71 (2002) 227–241.
[2] S. Wang, G.Q. (Max) Lu, G.J. Millar, Energy Fuel 10 (1996) 896–904.
[3] R.W. Howarth, R. Santoro, A. Ingraffea, Clim. Change 106 (2011) 679–690.
[4] D. Pakhare, J. Spivey, Chem. Soc. Rev. 43 (2014) 7813–7837.
[5] M. Usman, W.M.A. Wan Daud, H.F. Abbas, Renew. Sustain. Energy Rev. 45 (2015) 710–744.
[6] J.M. Lavoie, Front. Chem. 2 (2014) 81.
[7] P.M. Mortensen, I. Dybkjær, Appl. Catal. A 495 (2015) 141–151.
[8] M.C.J. Bradford, M.A. Vannice, Appl. Catal. A 142 (1996) 73–96.
[9] Z. Shang, S. Li, L. Li, G. Liu, X. Liang, Appl. Catal. B 201 (2017) 302–309.
[10] N. Laosiripojana, S. Assabumrungrat, Appl. Catal. B 60 (2005) 107–116.
[11] S. Ali, M.J. Al-Marri, A.G. Abdelmoneim, A. Kumar, M.M. Khader, Int. J. Hydrogen Energy 41 (2016) 22876–22885.
[12] S. Wang, G.Q.M. Lu, Appl. Catal. B 16 (1998) 269–277.
[13] M.C.J. Bradford, M.A. Vannice, Catal. Rev. 41 (1) (1999) 1–42.
[14] D. Chen, R. Lødeng, A. Anundskås, O. Olsvik, A. Holmen, Chem. Eng. Sci. 56 (2001) 1371–1379.
[15] Y. Li, D. Li, G. Wang, Catal. Today 162 (2011) 1–48.
[16] J. Guo, H. Lou, H. Zhao, D. Chai, X. Zheng, Appl. Catal. A 273 (2004) 75–82.
[17] J.W. Han, J.S. Park, M.S. Choi, H. Lee, Appl. Catal. B 203 (2017) 625–632.
[18] V. Yu. Bychkov, Yu. P. Tyulenin, A.A. Firsova, E.A. Shafranovsky, A. Ya. Gorenberg, V.N. Korchak, Appl. Catal. A 453 (2013) 71–79.
[19] V.C.H. Kroll, H.M. Swaan, C. Mirodatos, J. Catal. 161 (1996) 409–422.
[20] V.C.H. Kroll, H.M. Swaan, S. Lacombe, C. Mirodatos, J. Catal. 164 (1997) 387–398.
[21] R.T.K. Baker, Carbon 27 (1989) 315–323.
[22] D. Chen, K.O. Christensen, E. Ochoa-Fernández, Z. Yu, B. Tøtdal, N. Latorre, A. Monzón, A. Holmen, J. Catal. 229 (2005) 82–96.
[23] A. Gohier, C.P. Ewels, T.M. Minea, M.A. Djouadi, Carbon 46 (2008) 1331–1338.
[24] Z. Li, M. Li, Z. Bian, Y. Kathiraser, S. Kawi, Appl. Catal. B 188 (2016) 324–341.
[25] C. Liu, J. Ye, J. Jiang, Y. Pan, ChemCatChem 3 (2011) 529–541.
[26] J. Zhang, F. Li, Appl. Catal. B 176–177 (2015) 513–521.
[27] Z. Li, L. Mo, Y. Kathiraser, S. Kawi, ASC Catal. 4 (2014) 1526–1536.
[28] J. Newnham, K. Mantri, M. Hassan, A. James, T. Suresh, K. Bhargava, Int. J. Hydrogen Energy 37 (2012) 1454–1464.
[29] E.C. Lovell, A. Fuller, J. Scott, R. Amal, Appl. Catal. B 199 (2016) 155–165.
[30] A. Kumar, A.S. Mukasyan, E.E. Wolf, Appl. Catal. A 401 (2011) 20–28.
[31] A. Kumar, A.S. Mukasyan, E.E. Wolf, Appl. Catal. A 372 (2010) 175–183.
[32] Y. Li, Y. Wang, X. Zhang, Z. Mi, Int. J. Hydrogen Energy 33 (2008) 2507–2514.
[33] M.C.J. Bradford, M.A. Vannice, Appl. Catal. A 142 (1996) 97–122.
[34] Ş.Ö. Özkara-Aydınoğlu, E. Özensoy, A.E. Aksoylu, Int. J. Hydrogen Energy 34 (2009) 9711–9722.
[35] J.J. Carberry, Chemical and Catalytic Reaction Engineering, McGraw-Hill, 1976.
[36] A.E. Castro-Luna, M.E. Iriarte, Appl. Catal. A 343 (2008) 10–15.
[37] M.M. Barroso-Quiroga, A.E. Castro-Luna, Int. J. Hydrogen Energy 35 (2010) 6052–6056.
[38] M. Montes, J.B. Soupart, M. de Saedeleer, B.K. Hodnett, B. Delmon, J. Chem. Soc. Faraday Trans. 11 (1984).
[39] W. Brockner, C. Ehrhardt, M. Gjikaj, Thermochim. Acta 456 (2007) 64–68.
[40] K.V. Manukyan, A. Cross, S. Roslyakov, S. Rouvimov, A. Rogachev, E.E. Wolf, A.S. Mukasyan, J. Phys. Chem. C 117 (2013) 24417–24427.
[41] J.R. Rostrup-Nielsen, J. Sehested, Adv. Catal. 47 (2002) 65–139.
[42] T. Borowiecki, Appl. Catal. 4 (1982) 223–231.
[43] H.S. Bengaard, J.K. Nørskov, J. Sehested, B.S. Clausen, L.P. Nielsen, A.M. Molenbroek, J.R. Rostrup-Nielsen, J. Catal. 209 (2002) 365–384.
[44] S. Takenaka, S. Kobayashi, H. Ogihara, K. Otsuka, J. Catal. 217 (2003) 79–87.
[45] D. Chen, K.O. Christensen, E. Ochoa-Fernández, Z. Yu, B. Tøtdal, N. Latorre, A. Monzón, A. Holmen, J. Catal. 229 (2005) 82–96.
[46] A.J. Cross, Ph.D. Thesis Chem. Biomol. Eng. University of Notre Dame, 2015.
[47] S.M. Bachilo, L. Balzano, J.H. Herrera, F. Pompeo, D.E. Resasco, R.B. Weisman, J. Am. Chem. Soc. 125 (2003) 11186–11187.
[48] V.R. Choudhary, S. Banerjee, A.M. Rajput, Appl. Catal. A 234 (2002) 259.
[49] J. Chen, R. Wang, J. Zhang, F. He, S. Han, J. Mol. Catal. A 235 (2005) 302–310.
[50] D.W. Schaefer, A.J. Hurd, Aerosol Sci. Tehcnol. 12 (1990) 876–890.
[51] F. Paulik, J. Paulik, M. Arnold, Thermochim. Acta 121 (1987) 137–149.
[52] R. Banerjee, P.A. Crozier, J. Phys. Chem. C 116 (2012) 11486–11495.